Supporting Information

Cascade Branch Migration-Triggered Strand Displacement Amplification for Specific and Sensitive Detection of MicroRNA

Yaxing Xie, [ab] Yulei Hou, [b] Yang Yu, [a] Jianhong Zhang, [b] Jinyan Long, [a] Mengqi Chen, [a] Xueqing Lang, [a] Xiaolan Yang*[a] and Hui Chen*[b]

a Key Laboratory of Medical Laboratory Diagnostics of the Education Ministry, College of Laboratory Medicine, Chongqing Medical University, Chongqing, 400016, PR China.

b Clinical Laboratories, The First Affiliated Hospital of Chongqing Medical University, Chongqing, 400016, PR China.

*Corresponding author:

Xiaolan Yang, Key Laboratory of Medical Laboratory Diagnostics of the Education Ministry, College of Laboratory Medicine, Chongqing Medical University, Chongqing, 400016, PR China; E-mail: xiaolanyang666@cqmu.edu.cn

Hui Chen, Clinical Laboratories, The First Affiliated Hospital of Chongqing Medical University, Chongqing, 400016, PR China; E-mail: huichen@cqmu.edu.cn

Experimental section

CBM-THCR assay A 50 μL of solution containing various concentrations of miR-155 was added to a 50 μL of solution containing 500 nM F/F-C double strands, and the mixed solution was incubated at room temperature for 30 min to produce FT. Next, 50 μL of the above solution containing FT was added to a 50 μL of solution containing 250 nM P1P2, and the mixed solution was incubated at room temperature for 30 min to produce FP1 and TP2. Then 50 μL of the above solution containing FP1 and TP2 was added to a 50 μL of solution containing 200 nM H1, H2, H3 and H4. Then the above 100 μL final solution was incubated at 25 °C for 90 min, and the fluorescence signal was detected on a Cary Eclipse fluorescence spectrophotometer (excitation wavelength: 490 nm; scanned range: 500 nm to 600 nm; excitation and emission slits: 5 nm each). DEPC-treated water containing 10 mM KCl and 2 mM $MgCl_2$ was used as the buffer system in the experiment.

Detection of miR-155 in human serum and human blood samples MiR-155 samples with various concentrations in DEPC-treated water were added to diluted normal human serum samples (diluted 20 times). Then the samples were involved in the detection strategy, and the recovery rate and relative standard deviation (RSD) were calculated. For the human blood samples, miRNAs were extracted from the blood of four breast cancer patients and four normal individuals by the miRNA Extraction Kit, and the extracted miRNAs were detected by the CBM-TSDA detection strategy to determine the concentration of miR-155. The human serum and whole blood samples were from the First Affiliated Hospital of Chongqing Medical University. This study follows the general principles set out in the Declaration of Helsinki, and it has been approved by the ethics committee of Chongqing Medical University (reference number: 2024021).

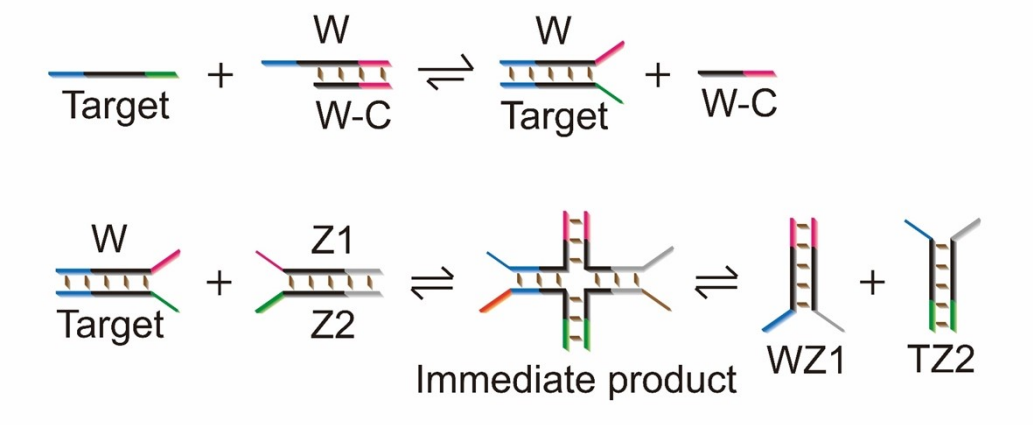

Fig. S1 Schematic of the CBM process. First, the W strand and the W-C strand (partial complementation with W) were added to the reaction system to form a double-stranded complex. Then the ssDNA target was added and proceeded with the TMSD to produce the W-Target Y-shaped probe. Subsequently, the W-Target Y-shaped probe proceeded with the double-stranded DNA branch migration in another reaction system with the Z1Z2 Y-shaped probe to produce the other two Y-shaped probes (WZ1 and TZ2) through the transition of the immediate state. The first-step TMSD reaction tended to produce the W-Target Y-shaped probe. The hybridization yield of the second-step double-stranded DNA branch migration was close to 50%, which tended to perform the optimal specificity. If there was a mutation site on the target, it would impede the production of the WZ1 and TZ2 Y-shaped probes. Due to the lack of the amplification process, the LOD of this method only reached the nanomolar level.

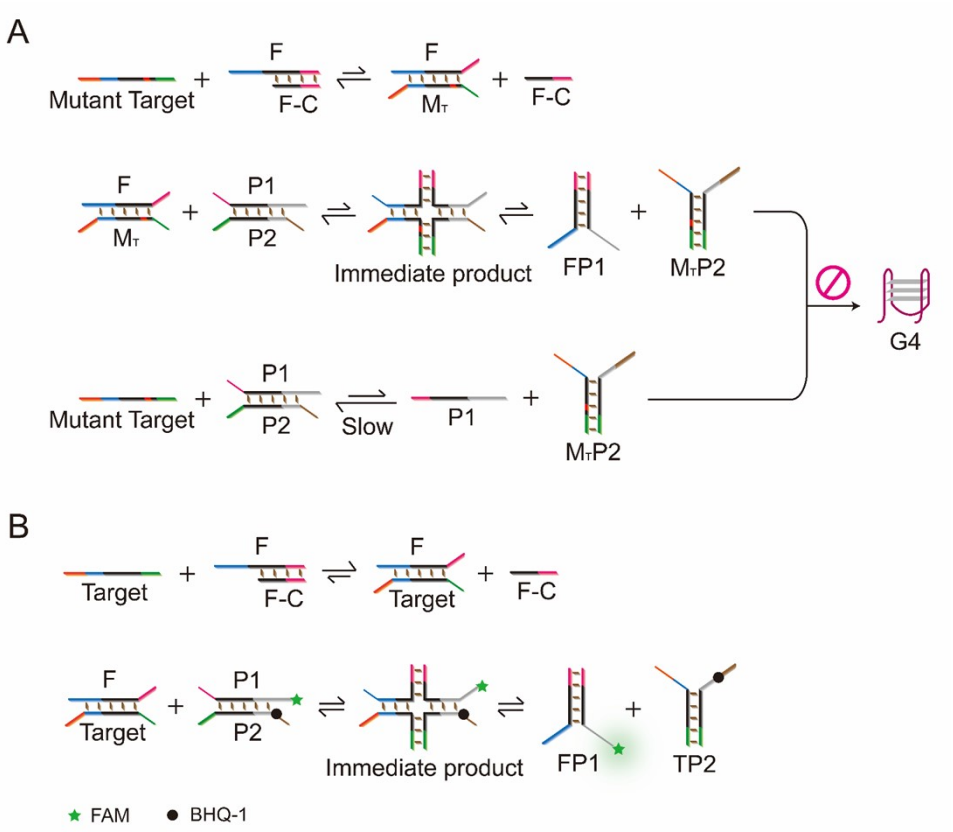

Fig. S2 (A) The CBM of the mutant target. Due to the presence of the mutation site, the formation of FM_T was inhibited. Similarly, the formation of FP1 and M_TP2 was inhibited. Meanwhile, the single-toehold DNA branch migration between the mutant target and P1P2 occurred accompanied with the double-stranded DNA branch migration, whose reaction rate is slower than the double-stranded DNA branch migration without the mutation site. Therefore, very few G4 products are produced eventually. (B) Detection principle of the fluorescence kinetics of the CBM. The FAM fluorophore and BHQ-1 fluorophore were labelled on the P1 and P2, respectively. Once FP1 and TP2 were produced, the distance between the FAM and the BHQ-1 increased, and the fluorescence signal increased significantly.

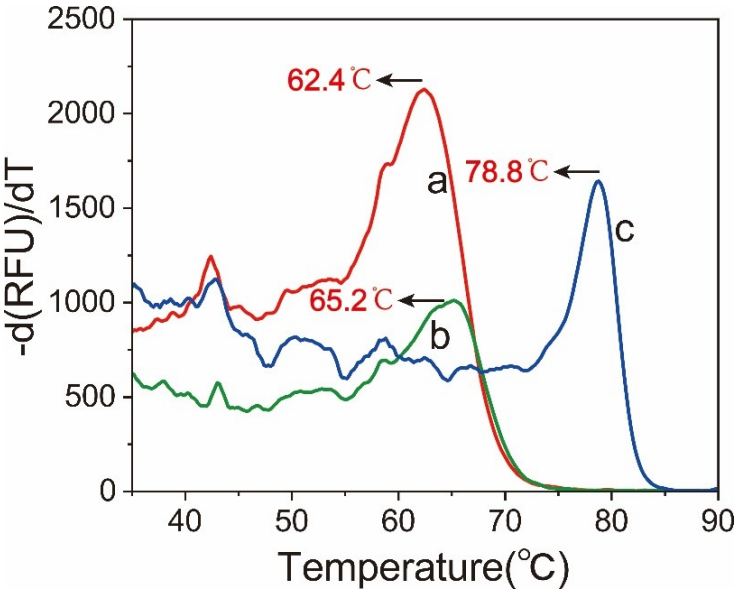

Fig. S3 Melting curve analysis of the formation of the TP2-L 3WJ structure: (a) TP2; (b) TP2-L; (c) TP2-L with KF. The first negative derivative plot [-d(RFU)/dT] was used to determine the melting temperature. The concentrations of the probes in the experiments were 500 nM each.

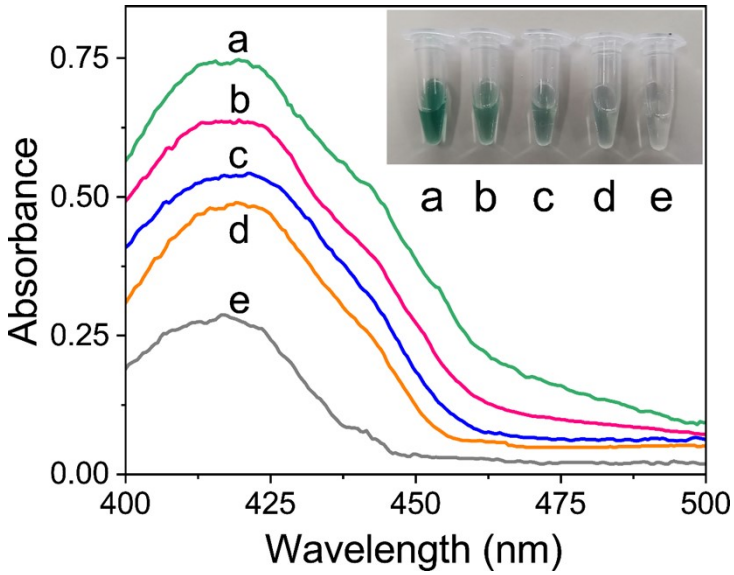

Fig. S4 UV-vis absorption spectra of the different samples: the concentration of miR-155 was (a) 25 nM; (b) 2.5 nM; (c) 250 pM; (d) 25 pM; (e) 0 pM. Inset: the corresponding photographs of the ABTS colorimetric analysis.

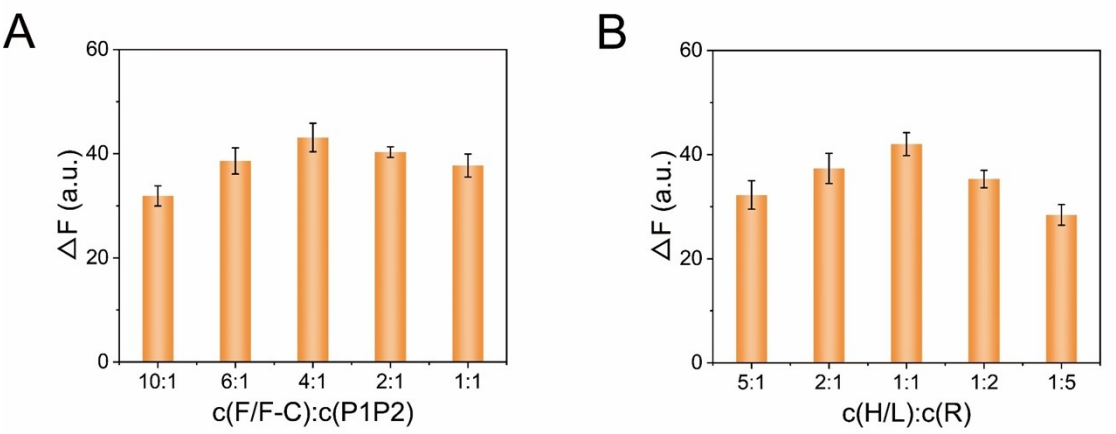

Fig. S5 Optimization of the concentration ratio of the probes: (A) Optimization of the concentration ratio of F/F-C and P1P2. The final concentration of F/F-C was set to 250 nM, and the concentration of P1P2 varies with the concentration ratio. (B) Optimization of the concentration ratio of H/L and R. The final concentration of H/L was set to 125 nM, and the concentration of R varies with the concentration ratio. The concentration of miR-155 was 250 pM. △F represents the difference between the experimental group and the control group. Error bars were derived from n=3 experiments.

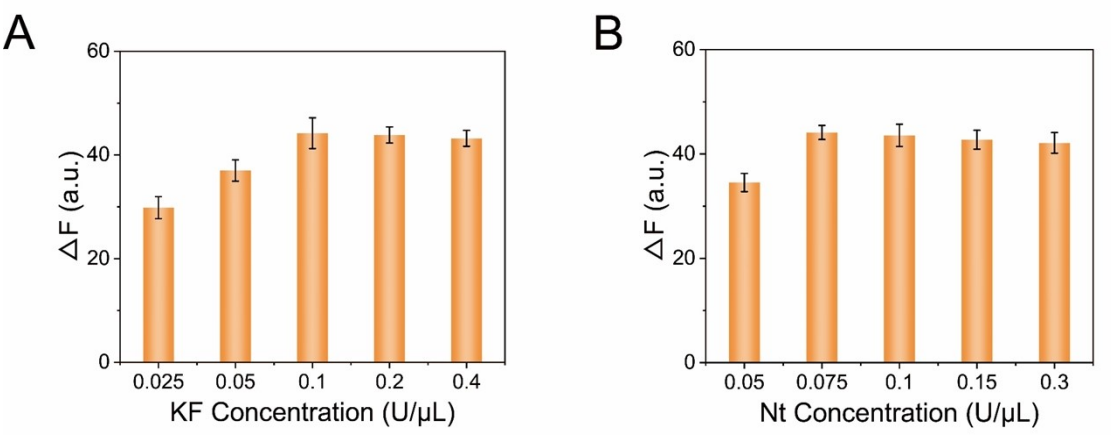

Fig. S6 Optimization of the concentrations of the enzymes: (A) Optimization of the KF concentration. (B) Optimization of the Nt concentration. The concentration of miR-155 was 250 pM. Error bars were derived from n=3 experiments.

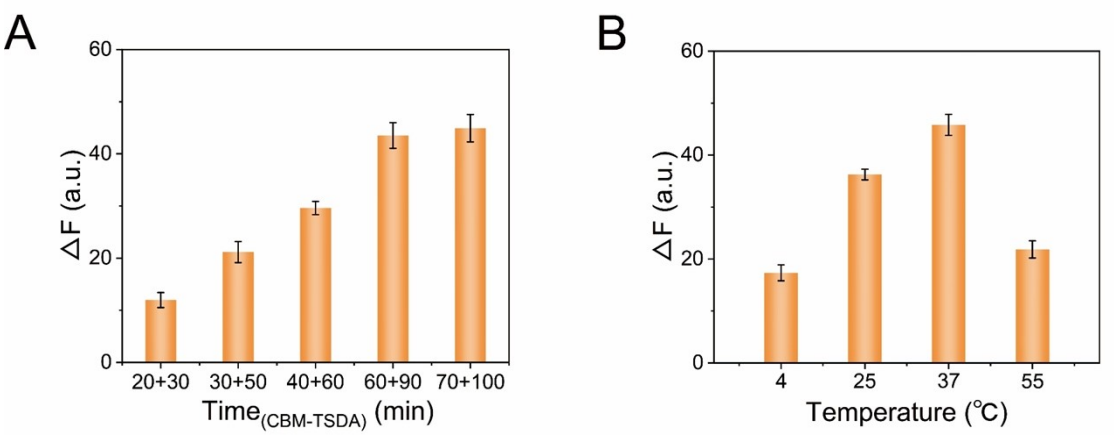

Fig. S7 Optimization of the reaction time of the CBM-TSDA, and the incubation temperature of the SDA: (A) Optimization of the reaction time of the CBM-TSDA. Before the "+" indicates the reaction time of the CBM, and the first-step TMSD and the second-step double-stranded DNA branch migration were set to split the reaction time of the CBM equally. After the "+" indicates the reaction time of the SDA. (B) Optimization of the incubation temperature of the SDA. Error bars were derived from n=3 experiments.

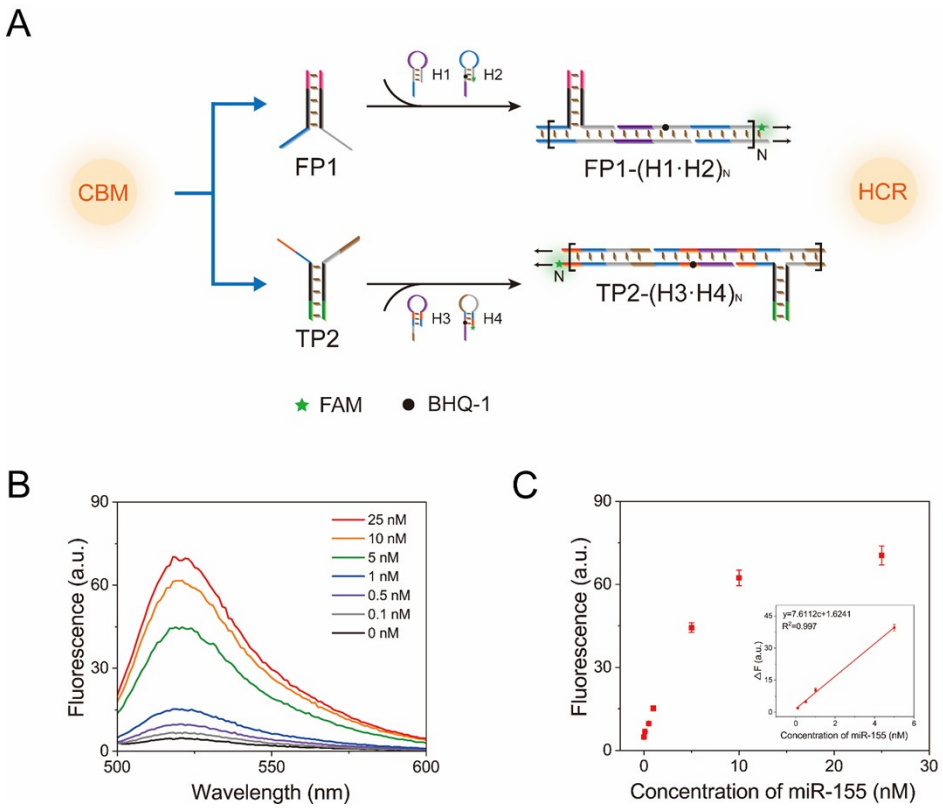

Fig. S8 (A) Schematic of the CBM-THCR. (B) Fluorescence emission spectra of the CBM-THCR in the presence of various concentrations of miR-155 ranging from 0 nM to 25 nM. (C) Fluorescence signal values of the CBM-THCR in the presence of various concentrations of miR-155 ranging from 0 nM to 25 nM (n=3). Inset displays the linear relationship between △F and the various concentrations of miR-155 ranging from 0.1 nM to 5 nM (n=3).

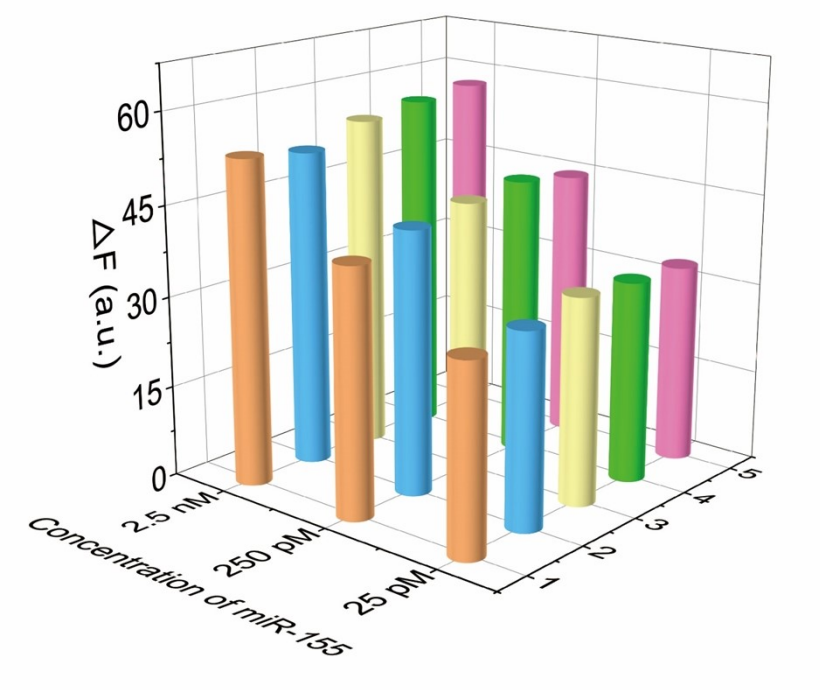

Fig. S9 Reproducibility of the detection strategy with 25 pM, 250 pM and 2.5 nM miR-155 for five independent experiments.

Table S1. Nucleic acid sequences used in the experiment.

No.	Sequence (5’ to 3’)
miR-155	UUAAUGCUAAUCGUGAUAGGGGU
F	CGGTTCTATCACGATTAGCATCAGT
F-C	TCGTGATAGAACCG
P1	AGTCAGAGTAATCGTGATAGAACCG
P2	ACCCCTATCACGATTACTCTTCCT
P1’	CAACAACAACAACAACAACAGTCAGAGTAATCGTGATAGAACCG
P2’	ACCCCTATCACGATTACTCTTCCTCCACCACCA
P1 (FAM)	FAM-AGTCAGAGTAATCGTGATAGAACCG
P2 (BHQ-1)	ACCCCTATCACGATTACTCdT (BHQ-1) TCCT
miR-155 (M1-1)	UUAAUGCUAAUUGUGAUAGGGGU
miR-155 (M1-2)	UUAAUGCUAAUCAUGAUAGGGGU
miR-155 (M1-3)	UUAAUGCUAAUCGUCAUAGGGGU
miR-155 (M2-1)	UUAAUGCUAAUCCUCAUAGGGGU
miR-155 (M2-2)	UUAAUGCUGAUCAUGAUAGGGGU
H	CTTAACTGTGTCTGGCTGAGGAGTGACTGATGCCACTCTGACT-P
L	CTTAACTGTGTCTGGCTGAGGCATAGGAAGAGACGCATTAA-P
M	TCAGCCAGACACAGTTAAG
R	TTCCCACCCTCCCACCCACCCGAGCTGAGGTACTTCTTAACTGTG TCTG-P
S	TCAGCTCGGGTGGGTGGGAGGGTGGGAA
H1	ACTGATGCCTCTGACTCCAGTGTCAGAGGC
H2	TGdT(FAM)CAGAGGCATCAGCCTCdT(BHQ-1)GACACTGGT

H3	AGGAAGAGGCATTAATCACGATAATGCCTC
H4	FAM-GATAATGCCTCTTCCTGGCATTAdT(BHQ-1)CGTGA

Note:

[1] The red markers indicate the mutation sites.

[2] The blue markers indicate the recognition sites of the Nt. BbVCI.

Table S2. Comparison of the detection strategy in this work with other miRNA detection strategies.

Detection strategy and target	Linearity range (M)	LOD (pM)	Specificity	References
Fluorescence (miR-21)	10^{-15}-5×10^{-11}	0.27×10^{-3}	Can discriminate miR-21 and other miRNAs	(Yin et al., 2017)
Electrochemistry (miR-155)	10^{-11}-10^{-4}	1.00	Can discriminate miR-155 and single-base mutation	(Tian et al., 2019)
Fluorescence (miR-21)	10^{-10}-10^{-7}	23.00	Can discriminate miR-21 and other miRNAs	(Zhao et al., 2020)
Fluorescence (miR-21)	5×10^{-11}-10^{-8}	1.00	Can discriminate miR-21 and single-base mutation	(Wang et al., 2020)
Fluorescence (let-7a)	2.5×10^{-11}-2.5×10^{-7}	9.01	Can discriminate let-7a and other let-7 family members	(Pu et al., 2021)
Electrochemistry (let-7a)	10^{-14}-5×10^{-8}	5.1×10^{-3}	Can discriminate let-7a and other let-7 family members	(Hua et al., 2022)
Fluorescence (miR-342-3p)	10^{-13}-5×10^{-11}	5.0×10^{-2}	Can discriminate miR-342-3p and single-base mutation with high DF	(Wijesinghe et al., 2022)
Fluorescence (miR-155)	5×10^{-13}-2.5×10^{-9}	0.28	Can discriminate miR-155 and single-base mutation with high DF	This work

Table S3. Detection of miR-155 in human serum with the developed strategy.

No.	Added target (pM)	Detected target (pM)	Recovery (%)	RSD (%, n=3)
1	5	5.34	106.8	2.4
2	50	48.70	97.4	4.3
3	500	476.14	95.2	3.8

References

1 Yin. H, Li. B, Zhou. Y, Wang. H, Wang. M and Ai. S, Biosens. Bioelectron., 2017, **96**, 106-112.

2 Tian. R, Ning. W, Chen. M, Zhang. C, Li. Q and Bai. J, Talanta, 2019, **194**, 273-281.

3 Zhao. X, Zhang. L, Gao. W, Yu. X, Gu. W, Fu. W and Luo. Y, ACS Appl. Mater. Interfaces., 2020, **12**, 35958-35966.

4 Wang. Z, Xue. Z, Hao. X, Miao. C, Zhang. J, Zheng. Y, Zheng. Z, Lin. X and Weng. S, Anal. Chim. Acta., 2020, **1103**, 212-219.

5 Pu. J, Liu. M, Li. H, Liao. Z, Zhao. W, Wang. S, Zhang. Y and Yu. R, Talanta, 2021, **230**, 122158.

6 Hua. X, Fan. J, Yang. L, Wang. J, Wen. Y, Su. L and Zhang. X, Biosens. Bioelectron., 2022, **198**, 113830.

7 Wijesinghe. K. M, Kanak. M. A, Harrell. J. C and Dhakal. S, ACS Sens, 2022, **7**, 1086-1094.